Analytical Modeling of a Novel High-Q Disk Resonator for Liquid-Phase Applications

Mohamad Sotoudegan, Stephen Heinrich, Fabien Josse, Nicholas Nigro, Isabelle Dufour, Oliver Brand

Analytical Modeling of a Novel High-Q Disk Resonator for Liquid-Phase Applications

Mohamad S. Sotoudegan,[1] Stephen M. Heinrich,[1] Fabien Josse,[2] Nicholas J. Nigro,[3] Isabelle Dufour,[4] Oliver Brand[5]

[1]Department of Civil, Construction and Environmental Engineering, Marquette University, Milwaukee, WI, USA

[2]Department of Electrical and Computer Engineering, Marquette University, Milwaukee, WI, USA

[3]Department of Mechanical Engineering, Marquette University, Milwaukee, WI, USA

[4]Université de Bordeaux, CNRS, Laboratoire de l'Intégration du Matériau au Système (IMS), Talence, France

[5]School of Electrical and Computer Engineering, Georgia Institute of Technology, Atlanta, GA, USA

ABSTRACT

To overcome the detrimental effects of liquid environments on MEMS resonator performance, the in-fluid vibration of a novel disk resonator supported by two electrothermally-driven legs is investigated through analytical modeling and the effects of the system's geometric/material parameters on the dynamic response are explored. The "all-shear interaction device (ASID)" is based on engaging the surrounding fluid primarily through shearing action. The theory comprises a continuous-system, multi-modal model and a single-degree-of-freedom model, the latter yielding simple formulas for the fundamental-mode resonant characteristics that often furnish excellent estimates to the results based on the more general model. Comparisons between theoretical predictions and previously published liquid-phase quality factor (Q) data (silicon devices in heptane) show that the theoretical results capture the observed trends and also give very good quantitative estimates, particularly for the highest-Q devices. Moreover, the highest Q value measured in the earlier study (304) corresponded to a specimen whose disk radius-to-thickness ratio was 2.5, a value that compares well with the optimal value of 2.3 predicted by the present model. The insight furnished by the proposed theory is expected to lead to further improvements in ASID design to achieve unprecedented levels of performance for a wide variety of liquid-phase resonator applications.

***Index Terms* – Liquid-phase MEMS resonators, quality factor, resonant frequency, disk microresonators, analytical modeling, vibrations.**

I. INTRODUCTION

Resonant devices based on micro/nanoelectromechanical systems (MEMS/ NEMS) span a broad spectrum of important applications, including chemical detection [1-7], biosensing [2-4, 6-10], rheological measurement [11-14], and energy harvesting [15-17]. However, many of these applications require liquid-phase operation, which poses significant challenges due to the drastic reduction in resonant frequency (f_{res}) and quality factor (Q) that is typically caused by the liquid's inertia and viscous energy dissipation [18-21]. Therefore, to overcome such challenges many investigators of MEMS/NEMS resonators for viscous fluid applications have focused on the use of unconventional vibration modes or novel device geometries. For example, to minimize coupling of the vibrating device with the surrounding viscous medium, researchers have explored the use of microcantilever structures vibrating in alternative modes, including higher modes of transverse (out-of-plane) flexure [8, 19, 22-24], in-plane flexure [25-33], axial deformation [25, 34, 35], and torsion [19, 22, 24, 26, 36-38]. Others have approached the problem by implementing cantilevers with embedded microfluidics [39] or in partial contact with the liquid [40]. Examples of novel geometries involving non-cantilever designs include a bridge beam supporting two half-disks [41], a trampoline structure vibrating in-plane [42], and a suspended plate that is in contact with liquid on one face only [43].

Another recent example of a novel disk-type microresonator for liquid-phase applications, introduced by Rahafrooz and Pourkamali [44, 45], is shown in Fig. 1a. The device is actuated electrothermally via two tangentially oriented legs, resulting in in-plane rotational oscillations of the disk as indicated schematically in Fig. 1b. The legs also serve as the motion-detection component since their axial strain results in a change in electrical resistance via the piezoresistive effect. (The reader is referred to [46] and [47] for more details regarding device

fabrication and the actuation/detection schemes.) This design differs from the previously mentioned devices in that virtually all of the surfaces of the device (disk and legs) move in a tangential direction, i.e., the device engages the surrounding liquid *through shearing action only*, which is expected to be a more efficient means of fluid-solid interaction [44, 45]. For this reason, we have referred to such a device as an "all-shear interaction device," or "ASID" [48-50]. Experimental data in [44, 45] have demonstrated proof-of-concept for the ASID design, as evi-

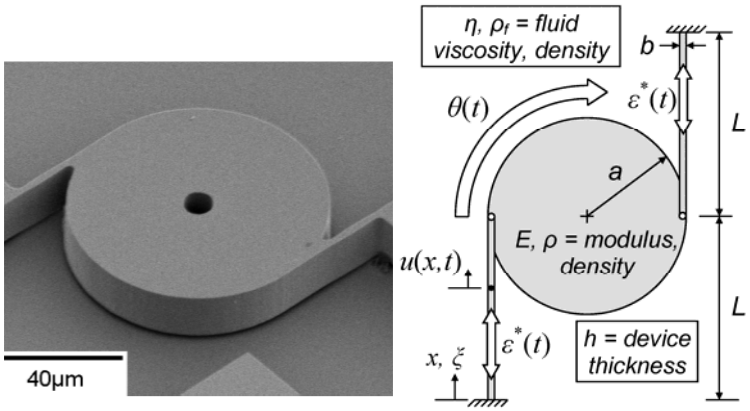

(a) **(b)**

Fig. 1: (a) Silicon-based disk MEMS resonator driven harmonically by imposed electrothermal axial strain in the legs [44, 45]; (b) Idealized model of the resonator depicting the concept of an "all-shear interaction device," or ASID [48-50].

denced by unprecedented levels of quality factor for a fully-immersed, liquid-phase device: $Q \approx 300$ in water [44] and in heptane [45]. Another potential advantage of the ASID in sensing applications is the potentially large functionalized surface area afforded by the disk.

While the experimental data presented in [44] and [45] are encouraging, the theoretical modeling included in those studies was limited to (undamped, in-vacuum) finite-element modal analyses. (The results of the simulations, i.e., the calculated mode shapes, were primarily used to confirm the hypothesis that shear is the dominant mode of interaction between the device and the

surrounding medium.) Therefore, in order to provide a more detailed and more general theoretical basis for the performance of the promising resonator design of [44] and [45], the purpose of the present paper is to perform analytical modeling with the aim of achieving a detailed theoretical understanding of how the various system parameters influence the ASID's dynamic response, including resonant characteristics. More specifically, the following objectives will be achieved in the present analytical investigation of an ASID resonator in a viscous fluid:

(1) A one-dimensional continuum model of a harmonically driven ASID will be derived and an explicit analytical solution (including multiple mode contributions) will be obtained. This model will incorporate the distributed nature of the leg mass, leg flexibility, actuation strain, and fluid resistance on the legs, as well as the inertia of the disk and the distributed fluid resistance on the disk.

(2) A simple single-degree-of-freedom (SDOF) model, based on neglecting the leg mass and fluid resistance on the legs, will be derived and solved for both the forced- and free-vibration cases. The latter case will result in simple, closed-form, approximate formulas for the in-liquid resonant characteristics of the device.

(3) The theoretical models of (1) and (2) will be employed to relate the dynamic response of the ASID to the geometric, material, and actuation parameters of the device, to provide guidelines for achieving optimal device geometries for maximizing Q and minimizing the fluid-induced decrease in f_{res}, and to investigate the range of applicability of the SDOF-based approximate formulas.

(4) The theoretical results of the present modeling effort will be validated by comparison with the existing Q data for ASID operation in heptane [45].

While the results to be presented herein are applicable to any liquid-phase application of an ASID microresonator, we emphasize that, within the specific context of MEMS sensing applications, significant improvements in resonant characteristics (Q and f_{res}) correspond to enhancements in sensor performance metrics such as mass or chemical sensitivity and limit of detection (e.g., [31, 51, 52]).

II. ANALYTICAL MODELING OF ASID

An idealized model of the physical device (the ASID) of Fig. 1a is shown in Fig. 1b. Also shown in Fig. 1b are the geometric and material parameters characterizing the idealized system. These include the disk radius a, the length L and width b of the legs, the device thickness h, the density ρ and Young's modulus E of the device material, and the density ρ_f and viscosity η of the surrounding fluid. The primary purpose of the present section is to mathematically formulate and solve the problem governing the in-fluid vibrations of the ASID when excited by harmonic electrothermal strains imposed on the two legs. Of ultimate interest is to understand how the resonant characteristics of the device, i.e., the resonant frequencies and quality factors associated with the various in-plane rotational modes, depend on the geometric and material parameters of the system. This will be achieved by employing a "continuous-system" or "distributed-parameter" modeling approach in Sect. II-A in which the distributed nature of the leg properties and the fluid resistance on the legs is considered. In addition a simple SDOF lumped-parameter model, in which the legs are treated as massless springs with no fluid resistance, is presented in Sect. II-B in an effort to obtain simple analytical expressions for the harmonic response and eigenproperties of the fundamental in-plane rotational mode.

A. CONTINUOUS-SYSTEM (DISTRIBUTED-PARAMETER) MODEL

The assumptions upon which the continuous-system model is based are the following: (1) the disk is rigid and has a solid circular geometry (i.e., the central hole of Fig 1a is neglected); (2) the supporting legs are elastic and treated as continuous axial members (i.e., bending and twisting are neglected); (3) each leg is fixed at one end and tangentially attached to the disk at the other end as shown in Fig. 1b; (4) the disk rotation is small; (5) the local fluid resistance (shear stress) on any surface of the device is approximated as that corresponding to the classical solution of Stokes's second problem for a harmonic, in-plane, translational oscillation of an infinite plane in a viscous fluid [53]; and (6) the legs are subjected to identical, electrothermally-induced, harmonic eigenstrains, $\varepsilon^*(t)$, which are uniform throughout the legs (Fig. 1b):

$$\varepsilon^*(t) = \varepsilon_0 e^{i\omega t} \ , \tag{1}$$

in which ε_0 is the amplitude of the imposed eigenstrain. In terms of the temperature change in the legs, $\varepsilon_0 = \Delta T \times CTE$, where ΔT is the temperature change amplitude and *CTE* denotes the coefficient of thermal expansion. Note that the imposed eigenstrain is a stress-free strain, while the total leg strain is the superposition of the eigenstrain and the elastic leg strain, the latter being associated with an axial stress in the legs.

The solution to Stokes's second problem implies that the fluid shear stress, τ, acting on a harmonically translating rigid planar surface may be expressed as a linear combination of the velocity, $\dot{D}$, and acceleration, $\ddot{D}$, of the surface, where D is the displacement of the surface and dots denote differentiation with respect to time t:

$$\tau = \bar{\bar{m}}_f \ddot{D} + \bar{\bar{c}}_f \dot{D} \ , \tag{2}$$

where

$$\bar{\bar{m}}_f = \sqrt{\frac{\rho_f \eta}{2\omega}}, \quad \bar{\bar{c}}_f = \sqrt{\frac{\omega \rho_f \eta}{2}} \tag{3a,b}$$

are the effective fluid mass and damping coefficients per unit area, respectively, and ω is the oscillation frequency of the surface. Employing assumption 5, the local fluid resistance at an arbitrary surface point of the ASID is approximated using the analog of Eq. (2) obtained by replacing D with the displacement magnitude of the surface point. Thus, $D = r\theta$ at any point on the disk surface, where r is the radial coordinate and θ the total disk rotation (measured from the position of zero leg strain). The extension of Eq. (2) for the shear stress at any point on the disk surface therefore becomes

$$\tau = \sqrt{\frac{\omega \rho_f \eta}{2}} \left(r\dot{\theta} + \frac{r}{\omega} \ddot{\theta} \right), \tag{4}$$

where ω is the actuation frequency and, thus, the steady-state oscillation frequency of the disk. An appropriate integration of Eq. (4) over the top and bottom (i.e., the circular areas) of the disk surface yields the resultant resisting torque due to the fluid in contact with these two surfaces:

$$T_{T+B} = -\pi a^4 \sqrt{\frac{\omega \rho_f \eta}{2}} \left(\dot{\theta} + \frac{1}{\omega} \ddot{\theta} \right). \tag{5}$$

The resisting torque on the lateral surface of the disk is obtained by multiplying the (uniform) shear stress on that surface, i.e., Eq. (4) evaluated at $r=a$, by the area of the lateral surface:

$$T_L = -2\pi a^3 h \sqrt{\frac{\omega \rho_f \eta}{2}} \left(\dot{\theta} + \frac{1}{\omega} \ddot{\theta} \right). \tag{6}$$

In addition the inertial torque associated with the disk mass, which opposes the rotational acceleration of the disk, is given by

$$T_I = \frac{\rho \pi a^4 h}{2} \ddot{\theta}. \tag{7}$$

In what follows a moment balance involving the fluid resistance torques and inertial torque, given by Eqs. (5)-(7) and shown in Fig. 2, will be incorporated into a boundary condition for the boundary value problem (BVP) governing the axial vibration of either leg.

Shifting the focus to the elastic deformation of an individual leg, an equilibrium analysis of an infinitesimal element of length dx may be performed (e.g., [54]), resulting in a differential equation governing the vibrating leg in the presence of the fluid:

$$\left[\rho bh + 2\overline{\overline{m}}_f (b+h)\right]\ddot{u}(x,t) + 2\overline{\overline{c}}_f (b+h)\dot{u}(x,t) - bh\sigma'(x,t) = 0 \ , \tag{8}$$

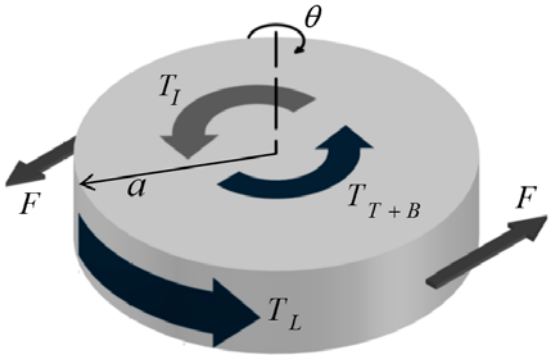

Fig. 2: Free-body diagram of vibrating disk showing inertial torque (T_I), total fluid resistance torque on the top and bottom faces (T_{T+B}), fluid resistance torque on the lateral surface (T_L), and forces exerted by the legs on the disk (F).

in which $u(x,t)$ and $\sigma(x,t)$ are the axial displacement and axial stress in the leg and the prime notation indicates differentiation with respect to x. The terms involving $\overline{\overline{m}}_f$ and $\overline{\overline{c}}_f$ account for the fluid resistance on the legs and have been introduced via a direct application of the Stokes result of Eq. (2). Note that the response quantity, $u(x,t)$, represents the *total* axial displacement, i.e., the superposition of the imposed (stress-free) electrothermal displacement and any elastic displacement that arises due to the dynamics of the problem. The axial stress is related to the *elastic* strain through Hooke's law; thus,

$$\sigma(x,t) = E\left[\varepsilon(x,t) - \varepsilon^*(t)\right] = E\left[u'(x,t) - \varepsilon_0 e^{i\omega t}\right], \tag{9}$$

where $\varepsilon(x,t)$ is the total axial strain in the leg. Substituting Eq. (9) into Eq. (8) leads to the following equation governing the axial displacement of the leg in a viscous fluid when excited by a uniform eigenstrain:

$$\left[\rho bh + 2\bar{\bar{m}}_f(b+h)\right]\ddot{u}(x,t) + 2\bar{\bar{c}}_f(b+h)\dot{u}(x,t) - Ebhu''(x,t) = 0 \ . \tag{10}$$

The equation of motion (10) must be accompanied by two boundary conditions reflecting the physical conditions at the ends of the leg. The fixed condition at x=0 is given by

$$u(0,t) = 0 \ , \tag{11}$$

while at x=L the disk exerts an axial force, F, on the leg. This second boundary condition may be written in terms of the axial stress at x=L as $\sigma(L,t) = F/bh$ or, using Eq. (9), as a condition on the displacement gradient at the disk-leg junction:

$$u'(L,t) = \frac{F}{Ebh} + \varepsilon_0 e^{i\omega t} \ . \tag{12}$$

Writing the rotational dynamic equilibrium equation for the free-body diagram of the disk shown in Fig. 2 enables one to express the force F in terms of the disk rotation θ. Rearranging this equation and relating the disk rotation to the end displacement of the leg via the kinematic relation, $\theta(t) = u(L,t)/a$, leads to

$$F = -\frac{\pi}{4}\rho h a^2 \left\{\left[1 + \left(1 + \frac{2h}{a}\right)\sqrt{\frac{2\rho_f \eta}{\rho^2 h^2 \omega}}\right]\ddot{u}(L,t) + \left(1 + \frac{2h}{a}\right)\sqrt{\frac{2\rho_f \eta\omega}{\rho^2 h^2}}\dot{u}(L,t)\right\} . \tag{13}$$

Placing Eq. (13) into Eq. (12) results in the explicit statement of the second boundary condition:

$$\frac{\pi}{4}\frac{\rho a^2}{Eb}\left\{\left[1 + \left(1 + \frac{2h}{a}\right)\sqrt{\frac{2\rho_f \eta}{\rho^2 h^2 \omega}}\right]\ddot{u}(L,t) + \left(1 + \frac{2h}{a}\right)\sqrt{\frac{2\rho_f \eta\omega}{\rho^2 h^2}}\dot{u}(L,t)\right\} + u'(L,t) = \varepsilon_0 e^{i\omega t} \ . \tag{14}$$

Equations (10), (11), and (14) constitute the BVP for the continuous-system model. Note that the actuation strain driving the system appears in the BVP only on the right-hand side of the second boundary condition, Eq. (14). Also note that the terms in Eq. (14) that are proportional to $\ddot{u}(L,t)$ and $\dot{u}(L,t)$ are frequency-dependent and correspond, respectively, to the portions of the end force due to (a) the rotational inertia of the disk and that of the fluid dragged by the disk and (b) the viscous torque exerted by the fluid on the disk. (See Fig. 2.)

For convenience the governing boundary value problem may be written in terms of a normalized axial displacement, $\bar{u} \equiv u / L$, dependent on dimensionless axial and time coordinates, $\xi \equiv x / L$ and $\bar{t} \equiv \omega_0 t$. The reference frequency ω_0 has been chosen as the in-vacuum fundamental axial frequency of a single leg of density ρ and Young's modulus *E*:

$$\omega_0 \equiv \pi\sqrt{E/\rho}/2L \ . \tag{15}$$

Letting primes and dots now denote differentiation with respect to ξ and $\bar{t}$, the BVP becomes

$$\bar{u}''(\xi,\bar{t}) - \frac{\pi^{3/2}}{2}\sqrt{\bar{L}_0\bar{L}}\left(1+\frac{1}{\bar{b}}\right)\sqrt{\bar{\omega}}\,\dot{\bar{u}}(\xi,\bar{t}) - \frac{\pi^2}{4}\left[1+\frac{2}{\sqrt{\pi}}\sqrt{\bar{L}_0\bar{L}}\left(1+\frac{1}{\bar{b}}\right)\frac{1}{\sqrt{\bar{\omega}}}\right]\ddot{\bar{u}}(\xi,\bar{t}) = 0 \ , \tag{16}$$

$$\bar{u}(0,\bar{t}) = 0 \ , \tag{17a}$$

$$\begin{aligned}\bar{u}'(1,\bar{t}) + \frac{\pi^3}{16}\frac{\bar{a}^2}{\bar{b}\,\bar{L}}\Bigg\{&\frac{2}{\sqrt{\pi}}\sqrt{\bar{L}_0\bar{L}}\left(1+\frac{2}{\bar{a}}\right)\sqrt{\bar{\omega}}\,\dot{\bar{u}}(1,\bar{t}) \\ &+\left[1+\frac{2}{\sqrt{\pi}}\sqrt{\bar{L}_0\bar{L}}\left(1+\frac{2}{\bar{a}}\right)\frac{1}{\sqrt{\bar{\omega}}}\right]\ddot{\bar{u}}(1,\bar{t})\Bigg\} = \varepsilon_0 e^{i\bar{\omega}\bar{t}} \ ,\end{aligned} \tag{17b}$$

in which the following dimensionless quantities have been defined:

$$\bar{\omega} \equiv \omega/\omega_0 \ , \quad \bar{a} \equiv a/h \ , \quad \bar{b} \equiv b/h \ , \quad \bar{L} \equiv L/h \ , \quad \bar{L}_0 \equiv L_0/h \equiv \sqrt{\rho_f{}^2\eta^2/E\rho^3}/h \ . \tag{18a-e}$$

Parameter L_0 is a "characteristic material length" which incorporates all of the model's material properties. Its normalized counterpart, $\overline{L}_0$, is the only material-dependent parameter appearing in the BVP described by Eqs. (16) and (17a,b).

One may easily show that the steady-state solution to the BVP due to the specified harmonic eigenstrain in the legs has the form

$$\overline{u}(\xi,\overline{t}) = \varepsilon_0 \overline{U}(\xi) e^{i\overline{\omega}\overline{t}} \ , \tag{19}$$

where

$$\overline{U}(\xi) = \frac{\sin\lambda\xi}{\lambda\cos\lambda - \dfrac{\pi^3\overline{a}^2\overline{\omega}^2\sin\lambda}{16\overline{b}\overline{L}}\left[1+2(1-i)\left(1+\dfrac{2}{\overline{a}}\right)\sqrt{\dfrac{\overline{L}_0\overline{L}}{\pi\overline{\omega}}}\right]} \ ,$$
$$\lambda = \frac{\pi\overline{\omega}}{2}\left[1+2(1-i)\left(1+\frac{1}{\overline{b}}\right)\sqrt{\frac{\overline{L}_0\overline{L}}{\pi\overline{\omega}}}\right]^{1/2} . \tag{20a,b}$$

Output signals of possible interest are the disk rotation, θ, which is identical to the average axial strain, ε_{avg}, in each leg, and the local axial strain at the supports, ε_{sup}. These signals are easily derived from the solution for the leg displacement. Convenient normalized forms of these output quantities are given by

$$\overline{\theta}(\overline{t}) \equiv \frac{\theta(\overline{t})}{\varepsilon_0 L/a} = \frac{\varepsilon_{avg}(\overline{t})}{\varepsilon_0 L/a} = \overline{U}(1)e^{i\overline{\omega}\overline{t}} , \qquad \overline{\varepsilon}_{sup}(\overline{t}) \equiv \frac{\varepsilon_{sup}(\overline{t})}{\varepsilon_0} = \overline{U}'(0)e^{i\overline{\omega}\overline{t}} . \tag{21a,b}$$

The mechanical signal given by Eq. (21a) corresponds to the overall electrical resistance in the legs and is thus the relevant output quantity for the device shown in Fig. 1a, whose motion detection scheme was based on the variations in the electrical resistance due to the piezoresistive effect [45]. On the other hand, the local strain signal represented by Eq. (21b) corresponds to the local electrical resistance whose changes would be monitored if the detection scheme were based on a piezoresistive Wheatstone bridge being employed near the support [30].

B. SINGLE-DEGREE-OF-FREEDOM (LUMPED-PARAMETER) MODEL

As a special case of the continuous-system model described in Section II-A, the resonator may be modeled as a single-degree-of-freedom (SDOF) system if the legs are assumed to behave as massless elastic springs experiencing no fluid resistance while all other assumptions of the previous section remain unchanged. With the normalized disk rotation, $\bar{\theta} = \bar{\theta}(\bar{t})$, being the only degree-of-freedom in this case, the SDOF equation of motion governing the model response may be deduced directly from Eq. (17b) by noting that the total strain in the legs is uniform in this case, i.e., $\bar{u}'(\xi, \bar{t}) = a\theta(\bar{t}) / L = \varepsilon_0 \bar{\theta}(\bar{t})$. Making this substitution into Eq. (17b) yields

$$\left[1 + \frac{2}{\sqrt{\pi}}\left(1 + \frac{2}{\bar{a}}\right)\sqrt{\bar{L}\bar{L}_0}\,\frac{1}{\sqrt{\bar{\omega}}}\right]\ddot{\bar{\theta}} + \frac{2}{\sqrt{\pi}}\left(1 + \frac{2}{\bar{a}}\right)\sqrt{\bar{L}\bar{L}_0}\,\sqrt{\bar{\omega}}\;\dot{\bar{\theta}} + \frac{16}{\pi^3}\frac{\bar{b}\,\bar{L}}{\bar{a}^2}\bar{\theta} = \frac{16}{\pi^3}\frac{\bar{b}\,\bar{L}}{\bar{a}^2}e^{i\bar{\omega}\bar{t}} \quad . \tag{22}$$

Note that Eq. (22) can also be obtained independently by considering dynamic equilibrium of all moments acting on the disk of Fig. 2, where the forces due to the legs are now given by $F = (bhE / L)(a\theta)$. The steady-state solution of Eq. (22) is given by

$$\bar{\theta}(\bar{t}) = \bar{\theta}_0 e^{i\bar{\omega}\bar{t}} \quad , \tag{23}$$

where $\bar{\theta}_0$ is the complex amplitude of $\bar{\theta} = \bar{\theta}(\bar{t})$ due to the imposed eigenstrain:

$$\bar{\theta}_0 = \frac{1}{1 - \dfrac{\pi^3}{16}\dfrac{\bar{a}^2}{\bar{b}\,\bar{L}}\bar{\omega}^2\left[1 + \dfrac{2(1-i)}{\sqrt{\pi}}\left(1 + \dfrac{2}{\bar{a}}\right)\sqrt{\bar{L}\bar{L}_0}\,\dfrac{1}{\sqrt{\bar{\omega}}}\right]} \quad . \tag{24}$$

One may also consider the free-vibration response of the SDOF model by setting the right-hand side of Eq. (22) to zero and interpreting the frequency parameter $\bar{\omega}$ appearing on the left-hand side as $\bar{\omega}_1$, defined as the normalized form of the in-fluid *natural* frequency (ω_1) of the SDOF system, i.e., $\bar{\omega}_1 \equiv \omega_1 / \omega_0$. (Subscript "1" denotes the first in-plane rotational mode of the device.) Assuming that $\bar{\omega}_1$ is insensitive to the damping term, the stiffness and frequency-

dependent mass coefficients in Eq. (22) result in the following frequency equation governing the unknown natural frequency parameter, $\bar{\omega}_1$:

$$\left(\sqrt{\bar{\omega}_1}\right)^4 + \frac{2}{\sqrt{\pi}}\left(1+\frac{2}{\bar{a}}\right)\sqrt{\bar{L}\bar{L}_0}\left(\sqrt{\bar{\omega}_1}\right)^3 - \frac{16}{\pi^3}\frac{\bar{b}\bar{L}}{\bar{a}^2} = 0 \ . \tag{25}$$

While Eq. (25) may easily be solved numerically for arbitrary values of the system parameters, we instead seek an analytical solution. Recognizing that the coefficient on the second term in Eq. (25) will be very small in many cases of practical interest (since $\bar{L}_0 \ll 1$ for micro-scale devices in most fluids), a truncated Taylor's series expansion of $\bar{\omega}_1$ in powers of this coefficient leads to the following approximate analytical formula for the in-fluid natural frequency parameter:

$$\bar{\omega}_1 \approx \frac{4}{\sqrt{\pi^3}}\left(\frac{\bar{b}\,\bar{L}}{\bar{a}^2}\right)^{1/2}\left[1-\frac{\pi^{1/4}}{2}\left(\frac{\bar{L}}{\bar{b}}\right)^{1/4}\left(\frac{2+\bar{a}}{\sqrt{\bar{a}}}\right)\sqrt{\bar{L}_0}\right] \ . \tag{26}$$

The form of Eq. (26) clearly indicates that the second term within the brackets represents the relative decrease in natural frequency caused by the fluid (relative to the in-vacuum case):

$$\left|\frac{\Delta\omega_1}{\omega_1}\right| \equiv \left|\frac{\omega_1-\omega_{1,vac}}{\omega_{1,vac}}\right| = \frac{\pi^{1/4}}{2}\left(\frac{\bar{L}}{\bar{b}}\right)^{1/4}\left(\frac{2+\bar{a}}{\sqrt{\bar{a}}}\right)\sqrt{\bar{L}_0} \ . \tag{27}$$

The quality factor, Q, associated with viscous dissipation in the fluid, is defined in terms of the viscous damping ratio, ζ, while from elementary vibration theory the latter may be related to the coefficients of the equation of motion (22) [54]. Evaluating those coefficients at the frequency given by Eq. (26) and neglecting higher-order terms results in the following estimate for Q based on the SDOF model:

$$Q_1 \equiv \frac{1}{2\zeta_1} \approx \frac{1}{\pi^{1/4}}\left(\frac{\bar{b}}{\bar{L}}\right)^{1/4}\frac{\sqrt{\bar{a}}}{2+\bar{a}}\frac{1}{\sqrt{\bar{L}_0}} \ , \tag{28}$$

where the "1" subscripts have been used to indicate that this result corresponds to the first mode of the resonator. The form of Eq. (28) permits a straightforward analysis of the effects that scaling of the device will have on Q. For example, if all dimensions of the ASID are increased (decreased) uniformly by a scaling factor α, the SDOF model predicts that the mode-1 quality factor will increase (decrease) by a factor of $\sqrt{\alpha}$. Similarly, if only the device thickness is increased (decreased) by a factor α while all other system parameters are held fixed, Eq. (28) implies that Q will increase (decrease), but the factor by which Q will change will depend not only on α but also on the disk radius. Both of these observations concerning scaling effects are consistent with the fact that the loss mechanism considered is essentially a surface effect; thus, any increase (decrease) in the volume-to-surface ratio of the device is expected to increase (decrease) Q.

A comparison of Eqs. (27) and (28) implies that the SDOF-based estimates for the fluid-induced relative decrease in natural frequency and the quality factor obey the following simple relationship, so that knowing one of these quantities permits the calculation of the other:

$$\left|\frac{\Delta\omega_1}{\omega_1}\right| = \frac{1}{2Q_1} \ . \tag{29}$$

Eq. (28) implies the existence of a relative maximum value for Q_1 with respect to disk size at the theoretically optimal value of $\bar{a} = 2$:

$$Q_{1,\max} = Q_1\big|_{\bar{a}=2} = \frac{\sqrt{2}}{4\pi^{1/4}}\left(\frac{\bar{b}}{\bar{L}}\right)^{1/4}\frac{1}{\sqrt{\bar{L}_0}} \ , \tag{30}$$

which, by Eq. (29), corresponds to a relative minimum in frequency drop:

$$\left|\frac{\Delta\omega_1}{\omega_1}\right|_{\min} = \left|\frac{\Delta\omega_1}{\omega_1}\right|_{\bar{a}=2} = \frac{1}{2Q_{1,\max}} \ . \tag{31}$$

The results presented by the authors in [49] show that, for a wide range of disk sizes, the SDOF free-vibration results given by Eqs. (26)-(28) are capable of providing excellent approximations to the resonant characteristics of the SDOF model (i.e., resonant frequency, vacuum-to-fluid drop in resonant frequency, and Q-factor at resonance) when driven harmonically. Therefore, in the next section these analytical results will be compared with the results of the more accurate continuous model of Sect. II-A to examine their range of applicability in the present context. As the forced-vibration resonant response is expected to reflect the underlying eigenproperties of the system in many cases, the approximate analytical results for mode 1 [Eqs. (26)-(31)] are expected to yield reasonable estimates of the corresponding resonant characteristics of the harmonically driven continuous model over appropriate ranges of system parameters. This will be explored in detail in the next section, as will be comparisons of experimental quality factor data and the theoretical predictions for Q.

III. RESULTS AND DISCUSSION

A. FREQUENCY RESPONSE

The normalized frequency response of the ASID can be obtained by evaluating Eqs. (20a,b) (continuous model) or Eq. (24) of the SDOF model over a range of actuation frequencies. While the SDOF model considers the disk rotation as the only output of the system (which is proportional to the leg strain, assumed to be uniform), the continuous model has been used to provide two outputs: the disk rotation (or average leg strain) and the local strain at the supports, as described earlier through Eqs. (21a,b). Since the focus of the present work is on the resonant characteristics of the ASID, we provide only sample frequency response curves for a specific set of system parameters as shown in Fig. 3 where the moduli (i.e., absolute values) of the complex functions $\bar{U}(1)$ and $\bar{U}'(0)$ of Eqs. (21a,b) and $\bar{\theta}_0$ of Eq. (24) are being evaluated as the

normalized response quantities. Physically, these response quantities correspond to normalized forms of either the disk rotation (average leg strain) amplitude or the local leg strain amplitude at the supports. The results displayed in Fig. 3 are based on a 20-μm-thick silicon ASID operating in heptane (ρ_f=679.5 kg/m^3, η=0.000386 Pa·s). Properties of silicon are taken as E=130 GPa and ρ=2330 kg/m^3, where the former value corresponds to the case in which the legs are aligned with the <100> direction [45, 55]. These data values yield a normalized characteristic material length of L_0 / h =3.2340e-07 which, unless indicated otherwise, will be used in all numerical results to

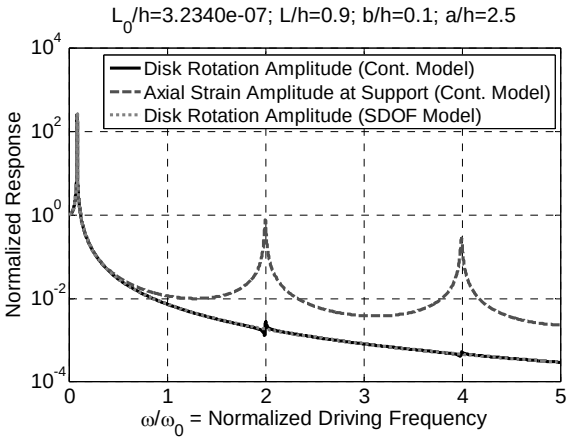

(a)

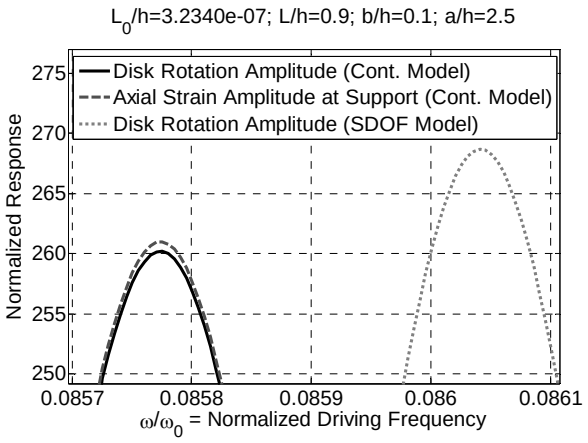

(b)

Fig. 3: (a) Theoretical output signals based on continuous model and SDOF model (20-μm-thick silicon ASID operating in heptane); (b) Zoomed view of signals for mode-1 response indicating slight difference between the two models.

follow; other specified geometric data will be noted directly on the figures. The continuous-model curves of Fig. 3 show that the two output signals have virtually identical responses in mode 1, while they tend to differ significantly in higher modes, with the local strain signal being stronger. As mentioned earlier in Section II-A, the disk rotation signal represents the average strain in the legs; thus, if the legs are excited in a mode other than the fundamental mode, some portions of the legs move in opposite directions, resulting in a smaller average strain in the leg. Moreover, the smaller value of disk rotation in the higher modes suggests that the boundary condition at the leg-disk junction is approaching a fixed condition; i.e., the disk inertia is limiting the disk rotation at higher driving frequencies. A comparison of the mode-1 results of the continuous and SDOF models shows that they are indistinguishable in Fig. 3a, while the zoomed view provided in Fig. 3b shows that the two models yield slightly different results. Nevertheless, for the case considered in Fig. 3 the SDOF model gives excellent approximations to the resonant frequency (0.3% high) and resonant peak amplitude (3% high).

B. RESONANT CHARACTERISTICS

The resonant frequencies of the system, defined as the exciting frequencies causing relative maxima in the plots of a response quantity versus the exciting frequency, can be extracted from the response curves generated by the continuous model or, for mode 1, by the SDOF model. Similarly, the corresponding quality factors may be extracted from the frequency response functions by employing the -3 dB bandwidth method [56] at each resonant peak. However, in what follows we focus only on the mode-1 resonant characteristics of the ASID as that mode is the most easily excited by the actuation method considered. In the results to be presented in what follows we shall denote the mode-1 resonant frequency as ω_{res} and mode-1

quality factor as Q. In addition to examining how the resonant characteristics depend on the system parameters, we will also compare the (forced-vibration) continuous-model results with the analytical expressions for the eigenproperties (free-vibration results) of the SDOF model. In all cases to be examined the disk rotation (average leg strain) signal [Eq. (21a)] will be employed as the continuous-model response quantity from which resonant characteristics are extracted, while all SDOF estimates of the resonant quantities will be based on the analytical expressions for the mode-1 natural frequency and quality factor [Eqs. (26)-(28)].

Figure 4 shows the dependence of the normalized mode-1 resonant frequency of the ASID on the normalized disk radius for a 20-μm-thick silicon device in heptane. Leg geometry values are fixed as indicated in the figure. Results extracted from the continuous model solution are shown in addition to those based on the SDOF-based analytical formula, Eq. (28). As the disk radius becomes larger the total effective mass of the system, including the contributions of the mass of the structure and the effective fluid mass, increases, as does the effective damping

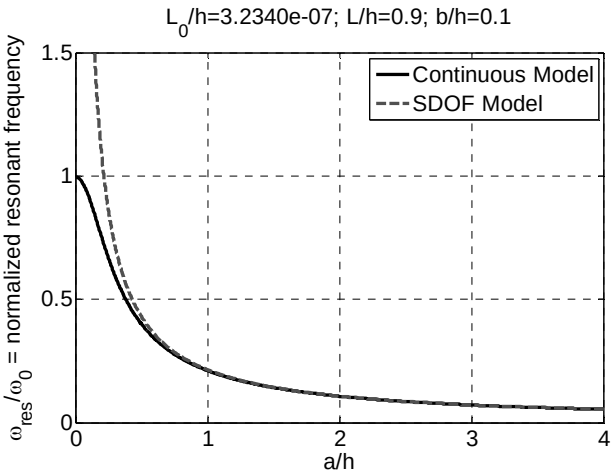

Fig. 4: Normalized mode-1 resonant frequency vs. normalized disk size. (20-μm-thick silicon ASID operating in heptane)

due to the increased contact area with the fluid. These two effects together cause the resonant frequency to drop significantly as *a/h* increases. It can also be seen in Fig. 4 that when the disk diameter exceeds the device thickness ($a/h>0.5$) the SDOF analytical result provides an excellent estimate for the resonant frequency as determined by the continuous model. However, for smaller disk radii the SDOF result may deviate significantly from the more exact result. This is due to the assumption in the SDOF model that the legs are massless, thereby resulting in a theoretically infinite natural frequency as the disk radius approaches zero. This behavior indicates that the SDOF formula should only be used for ASIDs having a sufficiently large disk radius. Also of note in Fig. 4 is the fact that the continuous-model curve begins at a value slightly smaller than unity, indicating that the resonant frequency of a cantilevered leg (with no disk attachment) in axial mode in fluid is very close to that of its in-vacuum counterpart, i.e., the leg-fluid shearing interaction is extremely efficient.

Variation of the *Q*-factor with respect to the normalized disk radius is shown in Fig. 5 for different values of L/h and a fixed value of b/h. Clearly seen in Fig. 5 is the existence of a relative maximum corresponding to an optimal disk size in each case. The SDOF model gives a constant optimal disk radius of $(a/h)_{opt}=2$ for all cases [see Eq. (30)], while this optimal value is seen to increase and depend on L/h (and b/h) when the more exact continuous model is used. Also of interest is that the continuous-model results show that the presence of the disk does not necessarily increase the *Q* value beyond that of the isolated leg ($a/h=0$) case, as indicated by the initial downward slope of the curves, but implementing a disk of optimal or near-optimal size may significantly improve *Q* over that of a simple cantilever driven axially. The figure also suggests that, in general, the accuracy of the SDOF estimate for *Q* [Eq. (28)] will deteriorate as the disk radius decreases and as the leg length increases. As mentioned earlier, this is due to the

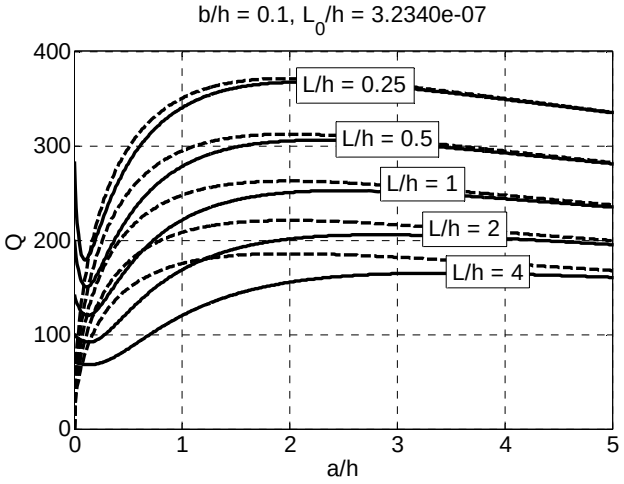

Fig. 5: Mode-1 quality factor vs. normalized disk size: continuous model (solid) and SDOF model (dashed). (20-µm-thick silicon ASID operating in heptane)

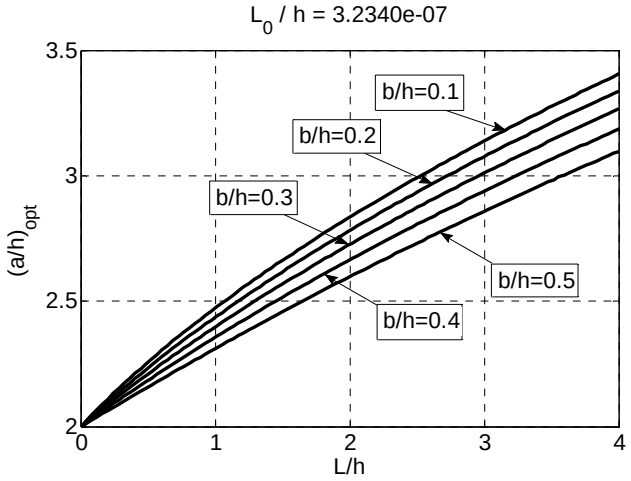

Fig. 6: Optimal disk size (resulting in maximum *Q*) versus the length and width of the legs. (20-µm-thick silicon ASID operating in heptane)

increasing importance of leg mass and leg fluid resistance (both neglected in the SDOF model) as the disk size decreases relative to the leg size.

The detailed variation of the optimal disk radius can be observed in Fig. 6 in which $(a/h)_{opt}$ increases with increasing L/h and decreases with increasing b/h. All curves begin at

the SDOF value of 2, indicating that the SDOF result provides a lower bound on the optimal disk size. While the results in Fig. 6 are associated with a particular device thickness and material system (20-μm-thick silicon device in heptane), additional calculations show that the dependence of the optimal value of a/h on the normalized material length, L_0/h, is negligible for practical ranges of solid and fluid properties and micro-scale device dimensions.

Figure 7 displays how the disk size changes the fluid-induced drop in the resonant frequency of the ASID for various values of L/h and fixed values of b/h and L_0/h. Of particular note is the relatively small value of relative frequency change due to the fluid. The continuous model shows that in all cases considered in the figure the surrounding liquid causes a decrease in the resonant frequency of less than 1%. Moreover, the optimal disk radius that yields a maximum Q value (see Figs. 5, 6) corresponds to a minimum value of the fluid-induced drop in the resonant frequency of the ASID. The same comments apply here regarding the trends in the accuracy of the SDOF analytical expression for the resonant frequency drop [Eq. (27)] as were made in the discussion of Fig. 5 and the SDOF formula for Q.

The maximum Q value corresponding to the optimal a/h value can be calculated for specified values of L/h, b/h, and L_0/h. These results are shown in Fig. 8 for both models, noting that L_0/h is fixed. As discussed earlier, the accuracy of the SDOF model becomes quite good as the legs become shorter. Moreover, the SDOF result [Eq. (30)] always provides an upper bound to the more accurate continuous-model result for the maximum Q, since the SDOF model neglects dissipation effects of the fluid in contact with the legs. Figure 8 demonstrates that the ASID is capable of unprecedented levels of Q in liquid (300-500 or even larger) if the legs are shorter and wider (i.e., stiffer) and if the disk radius is optimal (or near-optimal). However, there

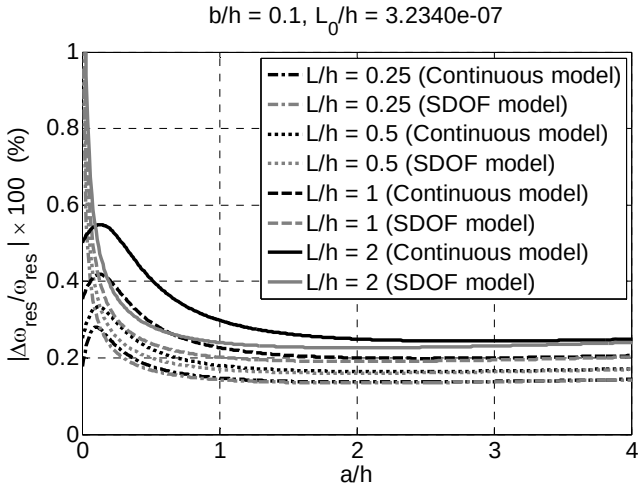

Fig. 7: Vacuum-to-fluid shift in resonant frequency vs. normalized disk radius. (20-µm-thick silicon ASID operating in heptane)

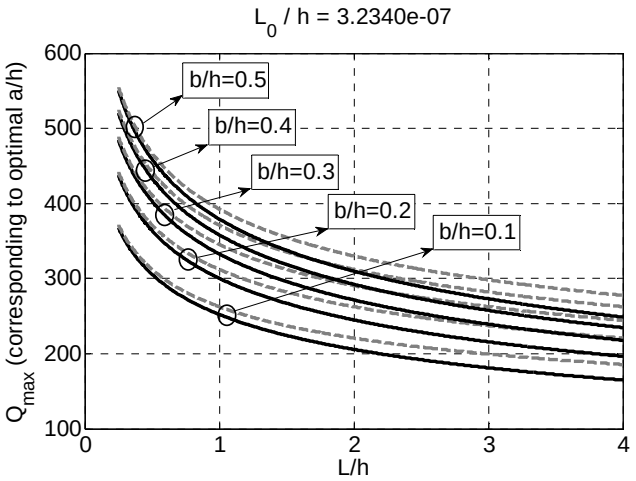

Fig. 8: Maximum *Q*-factor associated with the optimal disk size: continuous model (solid), and SDOF model (dashed). (20-µm-thick silicon ASID operating in heptane)

exist limitations that make an increase in leg stiffness beyond a certain level impractical as this could lead to an undetectable output signal. For example, if the legs are stiffened by decreasing their length, this will be accompanied by a reduction in the quasi-static disk rotation due to the electrothermal leg strain, since the quasi-static disk rotation is proportional to the leg length. In

addition, any stiffening of the legs, due to either decreasing L or increasing width b, would result in a reduction of the dynamic response of the system.

While all of the numerical results presented thus far have been based on silicon devices in heptane, the theoretical models may be used to study the effects of varying the structural material and/or the surrounding fluid. For example, one would expect the quality factor to vary considerably when the ASID is immersed in different liquids. This is explored in Fig. 9, in which

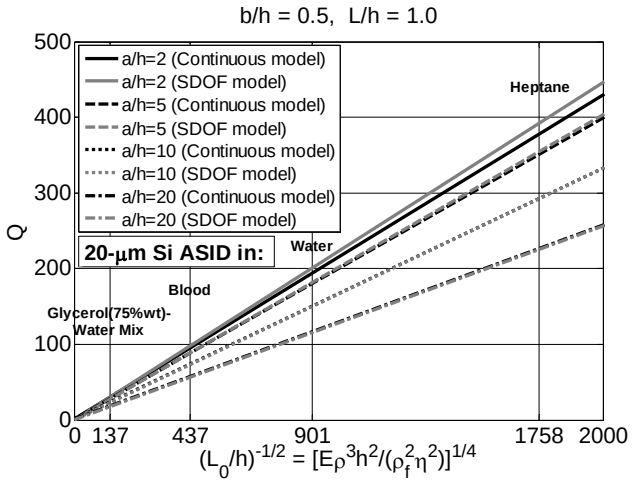

Fig. 9: Q-factor variation as a function of normalized material (solid/liquid) parameter. Particular device/fluid systems are show for illustrative purposes.

the effect of material properties (both liquid and solid) on Q for different values of a / h and fixed values of L / h and b / h is shown. The only parameter that is material-dependent is the abscissa quantity, $(L_0 / h)^{-1/2}$. It is apparent that the results of the continuous model yield an essentially linear variation of Q with respect to $(L_0 / h)^{-1/2}$, a result which was mathematically evident in the SDOF approximate relationship encapsulated by Eq. (28). Again, we see the expected departure of the SDOF results from those of the continuous model (a very slight overestimation in this case) as the disk size becomes smaller relative to the device thickness. As

expected, the device will resonate with sharper peaks (higher Q) in liquids having lower values of viscosity and density; Q will also increase as the device density or modulus is increased. (See the material-dependence of the abscissa in Fig. 9.)

While the curves of Fig. 9 are general in the sense that they apply to arbitrary material properties and device thicknesses, we have indicated for illustrative purposes specific abscissa values corresponding to a 20-μm-thick silicon device immersed in four different liquids. Heptane, being the least viscous of the four liquids, gives the highest quality factor, whereas liquids of higher viscosity and density such as a glycerol (75%wt)-water mixture (ρ_f=1200 kg/m^3, η=0.036 Pa·s [57]) or blood (ρ_f=1060 kg/m^3, η=0.004 Pa·s [58]) are seen to reduce the quality factor significantly. Theoretical results such as those depicted in Fig. 9 may be useful in extrapolating experimental Q data for one material system (e.g., a Si device in water) to another material system (e.g., an SU-8 device in blood).

C. COMPARISON OF THEORETICAL QUALITY FACTOR PREDICTIONS WITH EXPERIMENTAL DATA

Our primary motivation for studying the mechanics of the ASID resonator was to understand how the system parameters influence the efficiency of vibration in liquid environments as measured by the quality factor Q. Therefore, to examine the validity of the theoretical models described in this paper a comparison will be made between the theoretical predictions for Q and the existing liquid-phase quality factor data presented in [45]. The data correspond to 23 specimens of designs similar to that shown in Fig. 1a, having a fixed leg width of b=2 μm and various values of device thickness and leg length. All devices were fabricated from silicon and measurements were made in heptane. (Details may be found in [44] and [45].) Property values used in the theoretical models for Si and heptane have been listed earlier in the

present paper. The value of L, the effective leg length in the models, is specified as indicated in Fig. 10. Finite element modal analyses for the mode of interest (first in-plane disk rotation mode) show that this dimension yields a good estimate of the distance over which the leg strain is primarily one-dimensional (axial); this choice is therefore consistent with model assumption (2) and with the dimension used in [45] to categorize the collected data. This latter point will facilitate the comparison which follows.

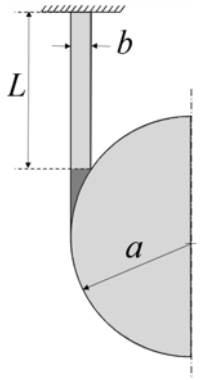

Fig. 10: Dimension used for the effective leg length L in modeling the ASID resonator.

The Q data of [45] and the predicted values based on the continuous and SDOF models are displayed in Fig. 11. An immediate and encouraging observation suggested by the comparison is that nearly all of the data (markers) are bounded by the corresponding range spanned by the theoretical results (continuous curves) and that these bounds are relatively tight, especially on the high-Q side which is of most practical interest. In addition the theoretical models capture the qualitative trends of the measured data quite well with respect to changes in both b/L and a/h. The models also provide very good quantitative estimates for Q in many cases, especially for the lower values of a/h which result in higher quality factors, i.e., the upper curves/markers in Fig. 11. In particular, the predicted Q values for the specimen that yielded the highest Q were within 3% of the measured result of 304. While no claims of optimizing the disk

size were made in [45], it is interesting that the specimen that yielded the largest Q value corresponded to the lowest ratio of a/h considered in that experimental study (a/h=2.5), while the present theory (Fig. 6), using that specimen's dimensions of (h, b, L)=(20, 2, 11) μm, predicts

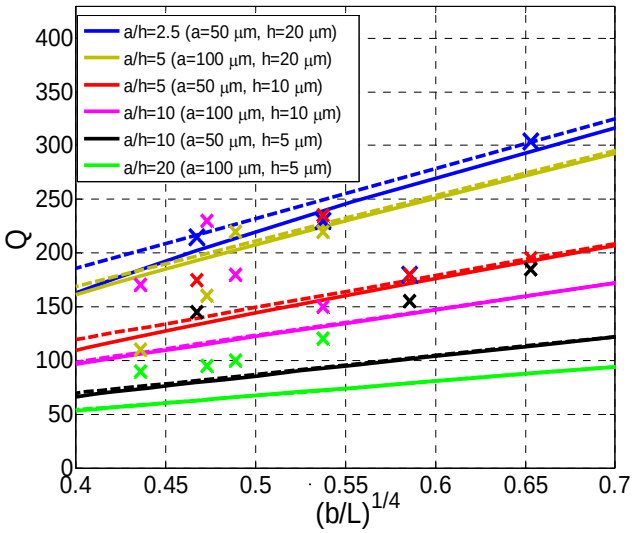

Fig. 11: Theoretical *Q*-factors (present study) vs. existing data for silicon specimens in heptane [45]. (Solid: continuous model; Dashed: SDOF model; X: experiment) [color online]

that $(a/h)_{opt} = 2.3$, which is consistent with the data. However, the quantitative difference between theory and experiment in Fig. 11 is significant for the higher a/h ratios of 10 and 20, for which the theoretical Q values are 30-50% below the data in 10 of 11 cases. Possible reasons for the quantitative discrepancy are the following: (1) The theoretical results are based on the use of a room temperature value of viscosity for heptane, i.e., reduction in viscosity due to temperature effects has not been included. (2) The model neglects the mass associated with the leg-disk junctions (see shaded portion in Fig. 10). Underestimating the mass will result in lower predicted Q values. (3) The model is based on the assumption of uniform electrothermal loading in the legs, a condition which may be difficult to achieve during testing. (4) Experimental error

associated with extraction of Q from noisy signals will obviously exist, as evidenced by the scatter of the data in Fig. 11. This error is expected to be higher for lower-Q signals.

If the two sets of theoretical curves in Fig. 11 are compared, one finds that, when the legs are shorter and/or the disk diameter is larger, the results of the SDOF analytical formula approach those of the continuous model, as expected, because the inertial and fluid effects associated with the legs become insignificant compared to those associated with the disk.

IV. SUMMARY AND CONCLUSIONS

A new analytical approach to a novel high-Q disk resonator supported by two tangential legs, described here as an "all-shear interaction device" or "ASID," has been explored through the use of two theoretical models: a continuous-system (distributed-parameter) model, which is capable of simulating multi-modal response, and the special case of a single-degree-of-freedom (SDOF) model, which is limited to the fundamental in-plane rotational mode. The SDOF model led to explicit analytical approximations for the resonant characteristics (resonant frequency, quality factor, and fluid-induced drop in the resonant frequency) of the ASID in terms of the system's geometric and material parameters. The SDOF analytical formulas have been compared with the resonant characteristics extracted from the frequency response curves of the more general multi-modal, continuous-system model. The analytical formulas were shown to be in very good agreement with the results of the more general model over a significant portion of the design space provided that the disk radius is sufficiently large relative to the device thickness. Both theoretical models indicate the existence of an optimal disk radius that maximizes the quality factor and minimizes the relative decrease in resonant frequency caused by the fluid. The SDOF model yields an optimal disk radius that is twice the device thickness [$(a/h)_{opt} = 2$]

regardless of leg dimensions, while the more refined model suggests that the optimal disk radius is slightly larger than the SDOF result [$(a/h)_{opt} > 2$] by an amount that depends on the size of the leg dimensions (length and width) relative to the device thickness. Both models suggest that ASID resonators are capable of achieving unprecedented levels of liquid-phase Q (300-500 or even higher) and fluid-induced resonant frequency reductions of less than 1%, and that such levels of performance are achievable if the ASID design includes relatively stiff (short and wide) legs and a disk of optimal (or near-optimal) size. The theoretical models also clearly show the effect of the liquid density and viscosity on the resonant characteristics of the device and thus enable one to map the performance measured in one liquid environment into resonant behaviors in other liquids without performing additional experiments in the other media.

The results of the present modeling effort have been validated by comparing the theoretical predictions for liquid-phase quality factor with published experimental data (measurements in heptane). The comparisons show that the models reproduce the trends exhibited by the existing data and give good quantitative estimates for Q, especially for those device geometries that exhibit the highest quality factors. In particular, both theoretical models yielded estimates within 3% of the highest Q measured in the data (Q=304); moreover, the specimen that achieved this level of resonant performance corresponded to a disk size of a/h=2.5, a value that was very close to the theoretically optimal value of $(a/h)_{opt} = 2.3$ given by the continuous model derived in this study. While most of the theoretical predictions for Q for larger disk sizes (a/h = 10 and 20) were 30-50% below the measured values, the quantitative agreement between theory and experiment was quite good for the higher-Q devices (a/h = 2.5 and 5) which are of most interest in resonator applications. These results suggest that the new analytical models presented herein may furnish a relatively simple, yet sufficiently accurate, theoretical

foundation for the encouraging performance of ASID-type devices in past experiments and may serve as the basis for a rational approach to designing these microresonators to achieve maximum performance in a wide variety of applications and liquid environments.

Acknowledgments

This work was supported in part by NSF Grant Nos. ECCS-1128992 and ECCS-1128554, The Graduate School of Marquette University, and the Marquette University Department of Civil, Construction and Environmental Engineering. The authors would also like to thank the reviewers for their suggestions for improving the paper.

References

[1] K.M. Goeders, J.S. Colton, and L.A. Bottomley, "Microcantilevers: Sensing Chemical Interactions via Mechanical Motion," *Chem. Rev.* **108**, no. 2, pp. 522-542 (2008).

[2] H. Campanella, *Acoustic Wave and Electromechanical Resonators*, Artech House, Norwood, MA (2010).

[3] H.K. Hunt and A.M. Armani, "Label-free biological and chemical sensors," *Nanoscale* **2**, pp. 1544-1559 (2010).

[4] A. Boisen, S. Dohn, S.S. Keller, S. Schmid, and M. Tenje, "Cantilever-like micromechanical sensors," *Rep. Prog. Phys.* **74**, 036101, 30 pp. (2011).

[5] S. Fanget, S. Hentz, P. Puget, J. Arcamone, M. Matheron, E. Colinet, P. Andreucci, L. Duraffourg, E. Myers, and M.L. Roukes, "Gas sensors based on gravimetric detection—A review," *Sens. Act. B: Chem.* **160**, pp. 804-821 (2011).

[6] K. Eom, H.S. Park, D.S. Yoon, and T. Kwon, "Nanomechanical resonators and their applications in biological/chemical detection: Nanomechanics principles," *Physics Reports* **503**, pp. 115-163 (2011).

[7] Q. Zhu, "Microcantilever Sensors in Biological and Chemical Detections," *Sensors and Transducers* **125**, no. 2, Feb., pp. 1-21 (2011).

[8] T. Braun, V. Barwich, M.K. Ghatkesar, A.H. Bredekamp, C. Gerber, M. Hegner, and H.P. Lang, "Micromechanical mass sensors for biomolecular detection in a physiological environment," *Phys. Rev. E* **72**, 031907, 9 pp. (2005).

[9] J.L. Arlette, E.B. Myers, and M.L. Roukes, "Comparative advantages of mechanical biosensors," *Nature Nanotechnology* **6**, April, pp. 203-215 (2011).

[10] B.N. Johnson and R. Mutharasan, "Biosensing using dynamic-mode cantilever sensors: A review," *Biosensors and Bioelectronics* **32**, pp. 1-18 (2012).

[11] N. Belmiloud, I. Dufour, A. Colin, and L. Nicu, "Rheological behavior probed by vibrating microcantilevers," *Appl. Phys. Lett*. **92**, no. 4, 041907, 3 pp. (2008).
[12] C. Riesch, E.K. Reichel, F. Keplinger, and B. Jakoby, "Characterizing Vibrating Cantilevers for Liquid Viscosity and Density Sensing," *J. Sensors* **2008**, 697062, 9 pp. (2008).
[13] I. Dufour, A. Maali, Y. Amarouchene, C. Ayela, B. Caillard, A. Darwiche, M. Guirardel, H. Kellay, E. Lemaire, F. Mathieu, C. Pellet, D. Saya, M. Youssry, L. Nicu, and A. Colin, "The Microcantilever: A Versatile Tool for Measuring the Rheological Properties of Complex Fluids," *J. Sensors* **2012**, 719898, 9 pp. (2012).
[14] I. Dufour, E. Lemaire, B. Caillard, H. Debéda, C. Lucat, S.M. Heinrich, F. Josse, and O. Brand, "Effect of hydrodynamic force on microcantilever vibrations:Applications to liquid-phase chemical sensing," *Sensors and Actuators B: Chemical* **192**, pp. 664-672 (2014).
[15] S.R. Anton and H.A. Sodano, "A review of power harvesting using piezoelectric materials (2003–2006)," *Smart Mater. Struct.* **16**, pp. R1-R21 (2007).
[16] S. Priya and D.J. Inman (eds.), *Energy Harvesting Technologies*, Springer, New York (2009).
[17] S. Beeby and N. White, *Energy Harvesting for Autonomous Systems*, Artech House, Norwood, MA (2010).
[18] J.E. Sader, "Frequency response of cantilever beams immersed in viscous fluids with applications to the atomic force microscope," *J. Appl. Phys.* **84**, no. 1, July, pp. 64-76 (1998).
[19] S. Basak, A. Raman, and S.V. Garimella, "Hydrodynamic loading of microcantilevers vibrating in viscous fluids," *J. Appl. Phys.* **99**, no. 11, 114906, 10 pp. (2006).
[20] C. Vančura, Y. Li, J. Lichtenberg, K.-U. Kirstein, A. Hierlemann, and F. Josse, "Liquid-Phase Chemical and Biochemical Detection Using Fully Integrated Magnetically Actuated Complementary Metal Oxide Semiconductor Resonant Cantilever Sensor Systems," *Anal. Chem.* **79**, no. 4, Feb., pp. 1646-1654 (2007).
[21] C. Vančura, I. Dufour, S.M. Heinrich, F. Josse, and A. Hierlemann, "Analysis of resonating microcantilevers operating in a viscous liquid environment," *Sens. Act. A: Phys.* **141**, pp. 43-51 (2008).
[22] C.A. Van Eysden and J.E. Sader, "Frequency response of cantilever beams immersed in viscous fluids with applications to the atomic force microscope: Arbitrary mode order," *J. Appl. Phys.* **101**, no. 4, 044908, 11 pp. (2007).
[23] M.K. Ghatkesar, T. Braun, V. Barwich, J.-P. Ramseyer, C. Gerber, M. Hegner, and H.P. Lang, "Resonating modes of vibrating microcantilevers in liquid," *Appl. Phys. Lett.* **92**, no. 4, 043106, 3 pp. (2008).
[24] B.N. Johnson and R. Mutharasan, "Persistence of bending and torsional modes in piezoelectric-excited millimeter-sized cantilever (PEMC) sensors in viscous liquids – 1 to 10^3 cP," *J. Appl. Phys.* ***109***, no. 6, 066105, 3 pp. (2011).

[25] I. Dufour, F. Josse, S.M. Heinrich, C. Lucat, C. Ayela, F. Ménil, and O. Brand, "Unconventional uses of microcantilevers as chemical sensors in gas and liquid media," *Sens. Act. B: Chem.* **170**, pp. 115-121 (2012).

[26] L.B. Sharos, A. Raman, S. Crittenden, and R. Reifenberger, "Enhanced mass sensing using torsional and lateral resonances in microcantilevers," *Appl. Phys. Lett.* **84**, no. 23, June, pp. 4638-4640 (2004).

[27] I. Dufour, S.M. Heinrich, and F. Josse, "Theoretical Analysis of Strong-Axis Bending Mode Vibrations for Resonant Microcantilever (Bio)Chemical Sensors in Gas or Liquid Phase," *JMEMS* **16**, no. 1, Feb., pp. 44-49 (2007).

[28] S.M. Heinrich, R. Maharjan, L. Beardslee, O. Brand, I. Dufour, and F. Josse, "An Analytical Model for In-Plane Flexural Vibrations of Thin Cantilever-Based Sensors in Viscous Fluids: Applications to Chemical Sensing in Liquids," *Proc., Int'l Workshop on Nanomechanical Cantilever Sensors*, Banff, Canada, May 26-28, 2 pp. (2010).

[29] S. Heinrich, R. Maharjan, I. Dufour, F. Josse, L.A. Beardslee, and O. Brand, "An Analytical Model of a Thermally Excited Microcantilever Vibrating Laterally in a Viscous Fluid," *Proc., IEEE Sensors 2010 Conf.*, Waikoloa, HI, Nov. 1-4, pp. 1399-1404 (2010).

[30] L.A. Beardslee, A.M. Addous, S.Heinrich, F. Josse, I. Dufour, and O. Brand, "Thermal Excitation and Piezoresistive Detection of Cantilever In-Plane Resonance Modes for Sensing Applications," *JMEMS* **19**, no. 4, Aug., pp. 1015-1017 (2010).

[31] L.A. Beardslee, K.S. Demirci, Y. Luzinova, B. Mizaikoff, S.M. Heinrich, F. Josse, and O. Brand, "Liquid-Phase Chemical Sensing Using Lateral Mode Resonant Cantilevers," *Anal. Chem.* **82**, no. 18, Sept., pp. 7542-7549 (2010).

[32] L.A. Beardslee, F. Josse, S.M. Heinrich, I. Dufour, and O. Brand, "Geometrical Considerations for the Design of Liquid-Phase Biochemical Sensors Using a Cantilever's Fundamental In-Plane Mode," *Sens. Act. B: Chem.* **164**, pp. 7-14 (2012).

[33] R. Cox, F. Josse, F., S.M. Heinrich, S., O. Brand, and I. Dufour, "Characteristics of laterally vibrating resonant microcantilevers in viscous liquid media," *J. Appl. Phys.* **111**, no. 1, 014907, 14 pp. (2012).

[34] C. Castille, I. Dufour, and C. Lucat, "Longitudinal vibration mode of piezoelectric thick-film cantilever-based sensors in liquid media," *Appl. Phys. Lett.* **96**, no. 15, 154102, 3 pp. (2010).

[35] R. Lakhmi, H. Debeda, I. Dufour, C. Lucat, and M. Maglione, "Study of Screen-Printed PZT Cantilevers Both Self-Actuated and Self-Read-Out," *Int'l J. Appl. Ceramics Tech.* **11**, no. 2, pp. 311-320 (2014).

[36] C.P. Green and J.E. Sader, "Torsional frequency response of cantilever beams immersed in viscous fluids with applications to the atomic force microscope,"*J. Appl. Phys.* **92**, no. 10, Nov., pp. 6262-6274 (2002).

[37] T. Cai, F. Josse, S. Heinrich, N. Nigro, I. Dufour, and O. Brand, "Resonant Characteristics of Rectangular Microcantilevers Vibrating Torsionally in Viscous Liquid Media," *Proc.,*

IEEE Int'l Freq. Control Symp. 2012, Paper 7175, Baltimore, MD, May 21-24, pp. 807-812 (2012).

[38] M. Aureli, C. Pagano, and M. Porfiri, "Nonlinear finite amplitude torsional vibrations of cantilevers in viscous fluids," *J. Appl. Phys.* **111**, no. 12, 124915, 16 pp. (2012).

[39] J.E. Sader, T.P. Burg, and S.R. Manalis, "Energy dissipation in microfluidic beam resonators," *J. Fluid Mech.* **650**, pp. 215-250 (2010).

[40] J. Linden and E. Oesterschulze, "Improving the quality factor of cantilevers in viscous fluids by the adaptation of their interface," *Appl. Phys. Lett.* **100***,* no. 11, 113511, 3 pp. (2012).

[41] J.H. Seo and O. Brand, "High *Q*-Factor In-Plane-Mode Resonant Microsensor Platform for Gaseous/Liquid Environment," *JMEMS* **17**, no. 2, Apr., pp. 483-493 (2008).

[42] P.S. Waggoner, C.P. Tan, L. Bellan, and H.G. Craighead, "High-Q, in-plane modes of nanomechanical resonators operated in air," *J. Appl. Phys.* **105**, no. 9, 094315, 6 pp. (2009).

[43] J. Linden, A. Thyssen, and E. Oesterschulze, "Suspended plate microresonators with high quality factor for the operation in liquids," *Appl. Phys. Lett.* **104**, no. 19, 191906, 3 pp. (2014).

[44] A. Rahafrooz and S. Pourkamali, "Rotational Mode Disk Resonators for High-Q Operation in Liquid," Waikoloa, HI, Nov. 1-4, pp. 1071-1074 (2010).

[45] A. Rahafrooz and S. Pourkamali, "Characterization of Rotational Mode Disk Resonator Quality Factors in Liquid," *Proc., 2011 IEEE Int'l Freq.Control Symp.* San Francisco, CA, May 1-5, 5 pp. (2011).

[46] A. Rahafrooz, A. Hajjam, B. Tousifar, and S. Pourkamali, "Thermal actuation, a suitable mechanism for high frequency electromechanical resonators," *Proc., IEEE MEMS Conf.*, Hong Kong, Jan. 24-28, pp. 200-203 (2010).

[47] A. Rahafrooz and S. Pourkamali, "Thermo-electro-mechanical modeling of high frequency thermally actuated I^2-BAR resonators," *Tech. Dig. Solid-State Sens.,Actuator Microsyst. Workshop*, Hilton Head Island, SC, June 2010, pp. 74-77 (2010).

[48] M.S. Sotoudegan, S.M. Heinrich, F. Josse, N.J. Nigro, I. Dufour, and O. Brand, "A Simple Model for the In-Plane Rotational Response of a Disk Resonator in Liquid: Resonant Frequency, Quality Factor, and Optimal Geometry," *Proc., 2013 Nanomechanical Sensing Workshop (NMC 2013)*, Stanford, CA, May 1-3, pp. 107-108 (2013).

[49] M.S. Sotoudegan, S.M. Heinrich, F. Josse, N.J. Nigro, I. Dufour, and O. Brand, "Effect of Design Parameters on the Rotational Response of a Novel Disk Resonator for Liquid-Phase Sensing: Analytical Results," *Proc., IEEE Sensors 2013 Conf.*, Baltimore, MD, Nov. 4-6, pp. 1164-1167 (2013).

[50] M.S. Sotoudegan, S.M. Heinrich, F. Josse, I. Dufour, and O. Brand, "A Multi-Modal Continuous-Systems Model of a Novel High-Q Disk Resonator in a Viscous Liquid," *Proc., 2014 Nanomechanical Sensing Workshop (NMC 2014)*, Madrid, Spain, Apr. 30-May 2, pp. 98-99 (2014).

[51] I. Dufour, F. Lochon, S.M. Heinrich, F. Josse, and D. Rebière, "Effect of Coating Viscoelasticity on Quality Factor and Limit of Detection of Microcantilever Chemical Sensors," *IEEE Sensors Journal* **7**, no. 2, Feb., pp. 230-236 (2007).
[52] R. Cox, F. Josse, M.J. Wenzel, S.M. Heinrich, and I. Dufour, "Generalized Model of Resonant Polymer-Coated Microcantilevers in Viscous Liquid Media," *Anal. Chem.* **80**, no. 15, Aug. 1, pp. 5760-5767 (2008).
[53] G. Stokes, "On the effect of the internal friction of fluids on the motion of pendulums," *Trans. Camb. Phil. Soc.* **9**, no. 2, pp. 8-106 (1851).
[54] R.W. Clough and J. Penzien, *Dynamics of Structures*, 2nd ed., McGraw-Hill, New York (1993).
[55] M.A. Hopcroft, W.D. Nix, and T.W. Kenny, "What is the Young's modulus of silicon?," *JMEMS* **19**, no. 2, Apr., pp. 229-238 (2010).
[56] J.H. Ginsberg, *Mechanical and Structural Vibrations*, John Wiley and Sons, New York (2001).
[57] N. Cheng, "Formula for the Viscosity of a Glycerol-Water Mixture," *Industrial and Engineering Chemistry Research* **47**, no. 9, pp. 3285-3288 (2008).
[58] J.D. Cutnell and K.W. Johnson, *Physics*, 8th ed., John Wiley and Sons, New York (2009).

Biographical Information of the Authors

Mohamad S. Sotoudegan received the B.S. degree in mechanical engineering from the Iran University of Science and Technology (IUST), Tehran, Iran, in 2011 and the M.S. degree in structural engineering from Marquette University, Milwaukee, WI, USA, in 2013. He is currently pursuing the Ph.D degree in structural mechanics at Marquette University where he is working on the vibration analysis of micro-scale resonators. He was recently a recipient of the Research Assistant Honors Award in 2014. His research interests lie in the areas of analytical/FEA modeling of the MEMS devices, solid-fluid interactions, and optimizing the microsystems performance.

Stephen M. Heinrich received the B.S. degree *summa cum laude* from Pennsylvania State University State, State College, PA, USA, in 1980 and the M.S. and Ph.D. degrees from the University of Illinois at Urbana-Champaign, Champaign, IL, USA, in 1982 and 1985, respectively, all in civil engineering. He joined the faculty of Marquette University, Milwaukee, WI, USA, as an Assistant Professor, where he was promoted to Professor of Civil Engineering in 1998. He was a recipient of the Reverend John P. Raynor Faculty Award for Teaching Excellence in 2000, Marquette's highest teaching honor. His research has focused on structural mechanics applications in microelectronics packaging and new analytical models for predicting and optimizing the performance of cantilever-based chemical/biosensors and, more recently, vibration energy harvesting devices. The investigations performed by him and his colleagues have resulted in over 100 refereed publications and three best paper awards from IEEE and the American Society of Mechanical Engineers.

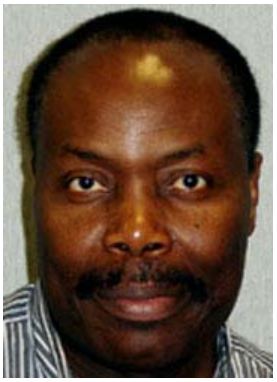

Fabien Josse (SM'–) received the License degree in mathematics and physics in 1976, and the M.S. and Ph.D. degrees in electrical engineering from the University of Maine, Orono, ME, USA, in 1979 and 1982, respectively. He has been with Marquette University, Milwaukee, WI, USA, since 1982, and is currently a Professor with the Department of Electrical and Computer Engineering, and the Department of Biomedical Engineering. His research interests include solid-state sensors, acoustic-wave sensors and microelectromechanical systems devices for liquid-phase biochemical sensor applications, investigation of novel sensor platforms, and smart sensor systems.

Nicholas J. Nigro was born in 1934. He received the B.S. degree in civil engineering from Michigan Technology University, Houghton, MI, USA, in 1956, and the M.S. degree in civil engineering from Iowa State University, Ames, IA, USA, in 1959. Following a three-year period as an Instructor at Southern Illinois University, Carbondale, IL, USA, he received the Ph.D. degree in theoretical and applied mechanics from the University of Iowa in 1965. He immediately began a distinguished 48-year career at Marquette University, Milwaukee, WI, USA, during which time he directed the research of over 80 master's and Ph.D. students, and was honored with six teaching awards, including the Marquette University Teaching Excellence Award in 1982. During the past six years, he served as a highly valued researcher as Professor Emeritus of Mechanical Engineering, interacting with students and faculty across the entire MU College of Engineering. His research portfolio spanned a diverse group of disciplines, including wave propagation, fluid-solid interaction, dynamics of high-altitude balloon systems, joining technology in electronic packaging, mechanics of liquid menisci, and, most recently, the modeling of microelectromechanical systems resonators. Since his unexpected passing in 2013, he has been sadly missed by a large community of family, friends, colleagues, and students whose lives he enriched.

Isabelle Dufour received the degree from the École Normale Supérieure de Cachan, Cachan, France, in 1990, and the Ph.D. and H.D.R. degrees in engineering science from the University of Paris-Sud, Orsay, France, in 1993 and 2000, respectively. She was a CNRS Research Fellow from 1994 to 2007, first in Cachan, working on the modeling of electrostatic actuators (micromotors and micropumps) and then, after 2000, in Bordeaux, working on microcantilever-based chemical sensors. She is currently a Professor of Electrical Engineering with the University of Bordeaux, Bordeaux, France. Her research interests are in the areas of microcantilever-based sensors for chemical detection, rheological measurements, and material characterization.

Oliver Brand (SM'–) is currently a Professor with the School of Electrical and Computer Engineering and the Executive Director of the Institute for Electronics and Nanotechnology with the Georgia Institute of Technology, Atlanta, GA, USA. He received the Diploma degree in physics from the Technical University of Karlsruhe, Karlsruhe, Germany, in 1990, and the Ph.D. degree from ETH Zurich, Zurich, Switzerland, in 1994. From 1995 to 1997, he was a Post-Doctoral Fellow with the Georgia Institute of Technology. From 1997 to 2002, he was a Lecturer with ETH Zurich and the Deputy Director of the Physical Electronics Laboratory.

Dr. Brand has co-authored over 190 publications in scientific journals and conference proceedings. He is a Co-Editor of the Wiley-VCH book series

Advanced Micro and Nanosystems, and an Editorial Board Member of *Sensors and Materials*. He served as the General Co-Chair of the 2008 IEEE International Conference on Micro Electro Mechanical Systems (MEMS), and has been a Technical Program Committee Member of the IEEE MEMS Conference, the IEEE Sensors Conference, and the Transducers Conference. He was a co-recipient the 2005 IEEE Donald G. Fink Prize Paper Award. His research interests are in the areas of integrated microsystems, microsensors, MEMS fabrication technologies, and microsystem packaging.